Effects of Sodium and Magnesium Ions on the Photochemically-

Induced Heterogeneous Formation of Manganese Oxides and their

Structural Evolution

Zhenwei Gao¹, Ping-I Chou¹, Byeongdu Lee², Yaguang Zhu¹, Deoukchen Ghim¹, and Young-Shin Jun^{1,*}

¹Department of Energy, Environmental and Chemical Engineering, Washington University in St. Louis, St. Louis, Missouri 63130, United States

²X-ray Science Division, Argonne National Laboratory, Argonne, Illinois 60439, United States

Address: One Brookings Drive, Campus Box 1180

E-mail: ysjun@seas.wustl.edu

Phone: (314) 935-4539

Fax: (314) 696-1223

The Journal of Physical Chemistry C (as part of The Journal of Physical Chemistry special virtual issue "Michael R. Hoffmann Festschrift")

Submitted: January 2023

Revised: May 2023

* To whom correspondence should be addressed

ABSTRACT: Manganese (Mn) oxides are abundant in aquatic and terrestrial environments, where they play significant roles in redox cycling and biological metabolisms. We recently observed that Mn oxides were homogenously formed during the abiotic oxidation of Mn²⁺(aq) to Mn(IV) by O₂ · via nitrate photolysis, at a rate comparable to that of biotic Mn oxides formation. On the other hand, for the heterogeneous formation of Mn oxides, the presence of a substrate can alter the required thermodynamic driving force, which may affect their crystalline phases and further influence the oxidative capability of redox cycling in environmental systems. However, little is known about the photochemically-induced heterogeneous formation of Mn oxides on substrates. In this study, we investigated the heterogeneous formation of Mn oxides on a quartz substrate in the presence of two environmentally abundant cations, Na⁺ and Mg²⁺. In contrast to homogeneously generated Mn oxides, the heterogeneously formed Mn oxides displayed earlier crystalline phase evolutions and morphological changes over time. Additionally, the coexistence of Na⁺ and Mg²⁺ ions greatly affected the initial crystalline phase and the phase evolution, as well 14 as the surface morphologies of the Mn oxides. These discoveries contribute to our understanding 15 of how various Mn oxides form in nature and provide insight into the processes involved in manufacturing specific Mn oxide crystalline structures for engineering applications.

1

2

3

4

5

6

7

8

9

10

11

12

13

INTRODUCTION

17

18

19

20

21

22

23

24

25

26

27

28

29

30

31

32

33

34

35

36

37

38

39

Manganese (Mn) oxides are one of the most reactive naturally occurring minerals, with more than 30 species in various geological settings. As electron donors and acceptors, they are important in redox cycling in environmental systems.²⁻⁴ Owing to the various oxidation states of Mn, its redox chemistry is significant in plant and human life, where it transfers electrons during metabolism.⁵, ⁶ Most natural Mn(III/IV) oxide solids are formed from the oxidation of Mn²⁺. However, Mn oxidation by O₂ is very slow and kinetically controlled.^{7, 8} Bacteria and fungi accelerate the oxidation of Mn²⁺(aq) to Mn(IV),⁹⁻¹¹ and bacteria-mediated Mn oxidation is believed to be the dominant oxidative pathway from Mn²⁺(aq) to Mn(IV) in natural systems. Abiotic, inorganic oxidation of Mn is considered less important than microbially-promoted processes because abiotic Mn²⁺(aq) oxidation has been thought to be very slow.^{7, 8} Previous studies reported the effects of mineral substrates on Mn oxidation as auto-catalysis, 12, 13 which promoted Mn oxidation by enhanced electron transfer. Surface-catalyzed abiotic oxidation resulted in Mn²⁺ half-lives ranging from 5 to 2800 days, depending on the presence and the type of mineral surfaces and the pH conditions. ¹⁴ However, this Mn oxidation proceeded mostly from Mn²⁺ to Mn(III). In surface water environments, photochemical processes trigger redox reactions in the cycling among aqueous Mn²⁺ and the solid phases of Mn(III) and Mn(IV). ¹⁵ In particular, we recently observed fast photochemically-assisted abiotic oxidation of Mn²⁺(aq) to Mn(IV) by reactive oxygen species (ROS) at rates comparable to those of biotic Mn oxidation. ^{16, 17} ROS formed during the photolysis of nitrate (i.e., completely inorganic systems) or the photolysis of dissolved natural organic matter (DOM) induced Mn oxidation. ¹⁶⁻¹⁸ In addition, in the presence of halide ions, such as Br⁻ and Cl⁻, reactive halogen species were formed, further promoting Mn oxidation. ^{18, 19} These results provide critical evidence for the fast abiotic formation of homogeneous Mn oxide in nature.

Heterogenous nucleation and growth occur in the presence of a substrate. Compared with homogeneous nucleation, heterogeneous nucleation can greatly influence the fate and transport of aqueous ions and mineral nucleation. The growth of the formed minerals is impacted by the electrostatic forces between the substrate and aqueous ions, and the newly formed minerals on the surface can affect the electrical properties of the surface. On the other hand, interfacial energies control the heterogeneous nucleation and growth, because the energy barrier to heterogeneous nucleation is affected by the substrate—water and precipitate—substrate interfacial energies. In addition, the hydrophilicity of the substrate can also change the energy barrier, affecting the nucleation and growth of the minerals.

The presence of the substrate and co-existing ions can also affect the crystalline structures of the formed minerals.^{27, 28} For example, quartz substrates behaved as an epitaxial host for the nucleation and growth of witherite (BaCO₃).²⁹ Photolysis of polystyrene nanoplastics produced ROS, resulting in the heterogeneous formation of Mn oxides on the nanoplastics, with different crystalline structures than those of homogeneously formed Mn oxides.³⁰ Regarding co-existing ions, the presence of sulfate promoted CaCO₃ heterogenous growth with less calcite formation than that without sulfate.³¹ Moreover, previous studies have shown that intercalated cations, such as Na⁺, K⁺, Ca²⁺, and Mg²⁺, affect homogeneously formed Mn oxide structures. In particular, compared with Na⁺, Ca²⁺ facilitated the formation of birnessite with a long-range order during the oxidation of Mn²⁺(aq) by *Bacillus* sp. Strain SG-1.³² Wang et al. (2015) reported that K⁺ was found in the middle of the interlayer of birnessite, while Mg²⁺ was located above Mn vacancies in the layers, resulting in different micromorphologies.³³ Furthermore, Mg²⁺ was important in forming stable 10-Å phyllomanganate in the phase transformation from birnessite to todorokite under high temperature and pressure.³⁴ Thus, it is important to comprehend how coexisting cations affect the

heterogeneous formation of photochemically-induced Mn oxides. All these previous findings emphasize the need to systematically investigate the crystalline structures and structural evolution of the heterogeneous nucleation of Mn oxides in the presence of environmentally abundant cations, which can affect their roles as water-oxidizing catalysts^{35, 36} and their oxidation capabilities^{37, 38} in both engineered and environmental processes.

To address this knowledge gap, here we examined the heterogeneous formation of Mn oxides on quartz in the presence of Na⁺ and Mg²⁺. Quartz is the most abundant substrate in the environment,³⁹ and Na⁺ and Mg²⁺ are abundant cations in aqueous environments.⁴⁰ By using grazing incidence wide-angle X-ray scattering (GIWAXS), we identified the phase evolution of newly formed Mn oxides in a nitrate solution exposed to simulated sunlight. Using atomic force microscopy (AFM) measurements, this work provided information on the evolution and morphology of nanoscale heterogeneously formed Mn oxides. To elucidate the roles of Na⁺ and Mg²⁺, we examined the initial crystalline phase, phase evolution, and surface morphology of the heterogeneously formed Mn oxides in the presence of these cations. Different crystalline structures of Mn oxide, such as romanechite, cryptomelane, groutellite, and groutite were formed over the phase evolutions under these above conditions. The findings provide a better understanding of the mechanism and phase evolution of Mn oxides in the environmental cycle of Mn and the abundance of Mn oxides in terrestrial and aquatic systems. Furthermore, cryptomelane and romanechite were used as molecular sieves, 41, 42 and battery electrode materials. 43, 44 Cryptomelane and groutellite were also employed as catalyst materials. 45, 46 Hence, this work also suggests a new, simple, and environmentally friendly method for synthesizing targeted Mn oxide crystalline structures such as cryptomelane, groutellite, and groutite.

EXPERIMENTAL SECTION

63

64

65

66

67

68

69

70

71

72

73

74

75

76

77

78

79

80

81

82

83

84

Chemicals. All chemicals used in this study were at least American Chemical Society grade. 87 Manganese chloride (MnCl₂, 97%, anhydrous) was purchased from Beantown Chemical Co. (NH, 88 USA). Sodium nitrate (NaNO₃, \geq 99.0%) was obtained from Avantor Performance Materials, Inc. 89 (PA, USA). Magnesium chloride hexahydrate (MgCl₂·6H₂O, 99%–102%), sodium chloride 90 (NaCl, > 99%), sodium hydroxide (NaOH, > 97%), acetone ($\ge 99.5\%$), denatured absolute ethanol 91 (200 proof), and isopropyl alcohol (>99%) were purchased from VWR International LLC (PA,

86

92

93

94

95

96

97

98

99

100

101

102

103

104

105

106

107

108

USA). Deionized (DI) water (resistivity $\geq 18.2 \text{ M}\Omega \cdot \text{cm}$, Barnstead Ultrapure water systems) was used to prepare the solutions for all experiments.

Substrate Preparation. Quartz (SiO₂) was selected as the model substrate for heterogeneous MnO₂ nucleation because it is one of the most abundant minerals in the earth's crust.³⁹ A large single crystal quartz wafer was bought from MTI Corporation (CA, USA). The crystal had an atomically flat polished (100) surface (roughness < 5 Å). The (100) surface of quartz is as common in the natural environment as other quartz surfaces with similar surface energies.⁴⁷ The quartz wafer was cut into 0.5 cm × 0.5 cm squares using a slow diamond saw (MTI Corp., CA). To remove organic matter, the cut quartz substrates were cleaned overnight in a mixed solution of concentrated sulfuric acid and Nochromix[®]. ²² The quartz substrates were then sonicated successively in acetone, ethanol, and isopropyl alcohol for 30 min each, rinsed three times with DI water, and stored in DI water. To ensure that the quartz substrates were clean, they were imaged using AFM, as shown in the Supporting Information, Figure S1. The quartz substrates were dried with high-purity nitrogen gas before use.

Photo-oxidation Experiments. To photochemically induce the heterogeneous nucleation of Mn oxides on a quartz substrate, a stock solution containing 0.1 mM MnCl₂ and 1 mM NaNO₃ was prepared. The solution pH was adjusted to 9.0 ± 0.1 by adding NaOH solution. During the

experiments, which were conducted in triplicate, the stock solution was refreshed about every hour to make sure the pH was above 8.5. Considering that the U.S. Environmental Protection Agency (EPA) water quality criterion for pH in freshwater ranges from pH 6.5 to 9, 48 our experimental pH is relevant to environmental systems. Solid Mn(OH)₂ does not form under these conditions, because it has a low saturation index (SI) of -1.20 and a solubility product constant (K_{sp}) of 1.6×10^{-13} . 49 No pH buffer was utilized in these experiments because aqueous Mn³⁺ can be formed as an intermediate product during the photo-oxidation reaction of Mn²⁺, and the buffer could complex with aqueous Mn³⁺, affecting Mn oxidation. 50

109

110

111

112

113

114

115

116

117

118

119

120

121

122

123

124

125

126

127

128

129

130

131

As shown in Figure 1a, the cleaned quartz substrates were pasted on a Kapton film and placed inside a custom-made quartz cuvette (external dimensions of 45 mm \times 12.5 mm). The substrates were placed in the cuvette vertically to minimize the chance of attachment of homogeneously nucleated Mn oxides falling under gravity. The prepared solution was continuously pumped into the cuvette (~2 mL/min), and the photochemical reaction was initiated in the quartz reactor by simulated solar light from a 450 W Xenon arc lamp (Newport 6279NS). The light was passed through flowing tap water, which both filtered out near-infrared light and cooled the reactor. The lamp spectrum is shown in Figure S2. The cuvette was held under irradiation for 20 hours, during which time individual quartz substrates were removed at 6, 12, and 20 hr. The pH change between the inlet and outlet was less than 0.1, so our experiment ran in a constant pH environment. Further, to investigate the effects of different cations (Na⁺ or Mg²⁺) on the nucleation and crystalline structure evolution of heterogeneously nucleated Mn oxides, NaCl or MgCl₂ was added to the solution, as shown in Table 1. The concentrations of Mg²⁺ and Na⁺ can vary across different water bodies. For example, seawater typically contains around 50 mM Mg²⁺, while river water contains less than 0.5 mM Mg²⁺.⁵¹ Similarly, Na⁺ concentrations can range from

above 400 mM in seawater to less than 0.5 mM in river water.⁵¹ In this study, we focused on the effect of 10 mM Mg²⁺ on the heterogeneous formation of Mn oxides. Our previous study showed that the kinetics and crystallinity of formed Mn oxides were significantly affected by the ionic strength.¹⁹ Thus, the solutions containing NaCl or MgCl₂ had the same ionic strength (IS) for comparison, and the experimental procedures remained the same as above.

Mn Oxides Solid Phase Characterization. The reacted quartz wafers were washed with DI water and dried with high-purity nitrogen gas. The formation of heterogeneous Mn oxides and their phase evolutions on quartz were observed with GIWAXS at Beamline 12-ID-B of the Advanced Photon Source (APS) in Argonne National Laboratory (IL, USA). As shown in Figure 1b, the quartz substrate was first aligned with the middle of the 13.3 keV X-ray beam (200 μm in width and 20 μm in height). Then the incident beam illuminated the quartz substrate for 1 second at an angle of 0.11°, which is slightly lower than the critical angle of the quartz substrate for total reflection. The beam, scattered by newly formed Mn oxides on the quartz substrate, was collected by a PerkinElmer 4k × 4k detector 200 mm away from the sample to determine the crystalline phases of the Mn oxides. The measured 2D scattering images were averaged radially to plot the intensity versus the scattering vector (q). The peak locations in the plot were compared with reference minerals to identify the mineral phases.

To visualize the Mn oxides nuclei on quartz, measure their heights, and determine their morphologies, we used AFM tapping mode in the air (Nanoscope V multimode SPM, Veeco Inc., NY). The AFM probe tips were made of $0.01-0.025~\Omega$ cm antimony (n)-doped Si (Model: RTESP, MPP-11100-10, Bruker Corp., MA). The cantilevers were 125 μ m long and 35 μ m wide, and the nominal tip radius was 8 nm. AFM images of an average of 20 different locations on each sample were analyzed using Nanoscope 7.20 software, provided by Veeco. The Mn oxidation states in the

Mn oxides (s) samples were identified by X-ray photoelectron spectroscopy (XPS, PHI 5000 VersaProbe II, UlvacPHI with monochromatic Al Kα radiation (1486.6 eV)). The C 1s peak (284.8 eV) was used as the reference peak. To determine the ratio of Mn(II), Mn(III), and Mn(IV), the Mn 3p spin orbit was fitted with Mn(II) (47.8 eV), Mn(III) (48.5 eV), and Mn(IV) (49.8 eV) by Gauss-Lorentz fitting methods. As shown in Figure S3, the above reference peak values were measured from reference samples of Mn(II) (MnO, Sigma Aldrich), Mn(III) (γ-MnOOH, from the Atikokan area of Ontario, Canada (Mineralogical Research Co.)), and Mn(IV) (β-MnO₂, Sigma Aldrich). The percentages of the Mn(II), (III), and (IV) in the total Mn were determined from the ratio of each specific Mn peak area to the total Mn peak area. The Mn average oxidation state of each sample was calculated by summing the products of the percentages for each oxidation state multiplied by the number of the oxidation state. The error range of these values was calculated based on the standard deviation of duplicate tests. High-resolution transmission electron microscopy (HR-TEM, JEOL-2100F field emission) was utilized to image the morphologies of formed Mn oxides on quartz. After the photochemical reaction, a small steel blade was used to gently scrape the Mn oxides from the quartz surface into DI water. A droplet of the solution was placed on an ultrathin lacey carbon film coated-Cu grid (LC400-Cu-UL, Electron Microscopy Science, PA) for imaging.

RESULTS AND DISCUSSION

155

156

157

158

159

160

161

162

163

164

165

166

167

168

169

170

171

172

173

174

175

176

177

Photochemically-induced Abiotic Heterogeneous Formation of Mn Oxides on Quartz. During nitrate photolysis, reactive oxygen species can form, including $O_2^{\bullet-}$ and ${}^{\bullet}OH$. In our previous studies ${}^{17, 19}$ of the photolysis of a solution containing 0.1 mM MnCl₂ and 1 mM NaNO₃ at initial pH 9, we showed that $O_2^{\bullet-}$ is responsible for the homogeneous formation of birnessite (δ -MnO₂) with a layer structure.

In the current work, using quartz as a substrate to study the heterogeneous formation, we show that the crystalline structure of Mn oxides can also be affected by altering the required thermodynamic driving force, which can be different from the structures of homogeneously formed Mn oxides. As shown in Figure 2 and S4, Mn oxide was heterogeneously nucleated on the quartz substrate, driven by the photolysis of solutions containing 1 mM NaNO₃ and 0.1 mM MnCl₂ at pH 9. The XPS and AFM results in Figure S4 indicated the formation of Mn oxide solids at 3 hr of reaction. However, the GIWAXS pattern of Mn oxides without any sharp peaks was observed. Thus, amorphous Mn oxides may form in the initial stages of the reaction. To investigate the phase evolution of the formed Mn oxides, we analyzed the crystalline phases of Mn oxides via GIWAXS at 6, 12, and 20 hr. Samples were measured from two orientations by 90 degrees (e.g., 6 hr and 6 hr R90) to get more scattering information. As shown in Figure S5, GIWAXS patterns with diffraction peaks of the clean quartz substrate are observed at q values of 1.50 and 1.88 Å^{-1} . As shown in Figure 2, at 6 hr, GIWAXS patterns show diffraction peaks at q values of 1.88~1.90 and 2.79 Å⁻¹, indicating that romanechite (American Mineralogist Crystal Structure Database (AMCSD) #0001198),⁵² with a 3×2 tunnel structure, was formed. The diffraction peaks for romanechite at q of 1.89 Å⁻¹ are stronger at 12 and 20 hr, suggesting the further formation and growth of romanechite. At 12 and 20 hr, new diffraction peaks are observed. The peak at a q value of 2.01~2.03 Å⁻¹ indicates the formation of cryptomelane (α-MnO₂, AMCSD #0009758),⁵³ with a 2×2 tunnel structure. In addition, the peak at a q of 2.24 Å⁻¹ suggests the formation of groutite (α -MOOH, AMCSD #0013941),⁵⁴ with a 2×1 tunnel structure. These results demonstrate the structural evolution of abiotically-formed Mn oxides on quartz during photolysis within a short period. In this study, the GIWAXS results were compared with the diffraction patterns of all Mn (hydr)oxides in the ICDD PDF-4 database, leading to the determination that romanechite,

178

179

180

181

182

183

184

185

186

187

188

189

190

191

192

193

194

195

196

197

198

199

cryptomelane, and groutite were the potential phases. However, it should be noted that not all of the characteristic peaks of cryptomelane and romanechite were observed in the GIWAXS patterns. Possibly, the Mn oxide particles preferentially grew in a few oriented directions on the quartz substrate, which would obscure some characteristic peaks. For nanoparticles, it is common for not all characteristic diffraction peaks to be observed. Also, the samples were measured using GIWAXS from only two orientations with respect to X-ray direction, which may have missed some of the characteristic peaks. In addition, the formation of Mn oxides was influenced by the presence of the quartz substrate, resulting in altered crystalline structures. Note that in the absence of the quartz substrate, homogeneous formation of birnessite (δ-MnO₂) occurred during the photolysis of a solution containing 1 mM NaNO₃ and 0.1 mM MnCl₂ at the initial pH 9, high contrasts with our observations of heterogeneous Mn oxides formation.

On the other hand, the XPS spectra in Figure 3 show that the Mn oxides in all the samples contained mostly Mn(IV) and Mn(III). From 6 to 20 hr, the Mn(IV) percentage decreases from $67.1 \pm 1.1\%$ to $56.5 \pm 2.1\%$, and Mn(III) percentage increases from $25.9 \pm 2.4\%$ to $41.7 \pm 1.8\%$, indicating that the crystalline structure evolution is accompanied by Mn oxidation state changes. The increase of Mn(III) in samples at 12 and 20 hr resulted from the formation of groutite (α -MOOH), which contains mostly Mn(III). The variations in the crystalline phases and oxidation states for Mn oxides can influence their oxidation capability,³⁷ and may further affect their oxidative activities in the environment.

Effects of Na⁺ and Mg²⁺ on the Crystalline Structures of Heterogeneously Formed Mn Oxides. Our study further investigated the effects of Na⁺ and Mg²⁺ on the crystalline structures of heterogeneously nucleated Mn oxides. As shown in Figure 4a, in the presence of Na⁺, GIWAXS patterns with diffraction peaks at q of 1.99~2.00 Å⁻¹ are observed at 6 hr, indicating that

cryptomelane was initially formed, which is different from the diffraction patterns without Na⁺ in Figure 2. From 6 to 12 hr, the formed cryptomelane (2×2 tunnel structure) evolved to romanechite (3×2 tunnel structure) and groutellite (AMCSD #0003566, ⁵⁶ with a 2×1 tunnel structure). At 20 hr, a very high intensity diffraction peak of romanechite at q of 1.90 $Å^{-1}$ is observed, suggesting its fast growth and increased crystallinity. On the other hand, as shown in Figure 4b, in the presence of 10 mM Mg²⁺, a tiny romanechite diffraction peak at 1.90 Å⁻¹ is observed at 6 hr. At 12 hr, the intensity of this diffraction peak is stronger, suggesting the formation and growth of romanechite. Additional peaks at q of 1.50 Å⁻¹ at 12 and 20 hr, and 2.23 Å⁻¹ at 20 hr are observed, indicating the formation of groutite. Moreover, at 20 hr, a peak at q of 2.00~2.01 Å⁻¹ suggests the formation of cryptomelane. The XPS spectra in Figure S6 provide evidence that Mg²⁺ is incorporated into Mn oxides at 20 hr. The above results clearly show that the presence of Na⁺ or Mg²⁺ affected both the initial crystalline phase and the phase evolution during the photochemically-induced heterogeneous nucleation and growth of Mn oxides on the quartz substrate. The crystalline structure evolution may result from the migration of Mn. A more detailed discussion about the tunnel structure evolution of Mn oxides is made in a later section.

224

225

226

227

228

229

230

231

232

233

234

235

236

237

238

239

240

241

242

243

244

245

246

Surface Morphology of Heterogeneously Formed Mn Oxides. We used AFM to investigate the surface morphology of heterogeneously formed Mn oxides. Figure 5 shows the representative images of statistical analyses of the surface morphologies of formed Mn oxides, made by taking at least an average of 20 locations for each sample. As shown in Figure 5a,d, without Na⁺ or Mg²⁺, both small and large pieces of heterogeneously nucleated Mn oxide particles were observed at 6 hr, with heights of up to 30 nm. From 6 to 20 hr, the large pieces gradually grew bigger, and a few narrow stripes of Mn oxides were also observed at 20 hr. In the presence of Na⁺ (Figure 5b,e), Mn oxide particles grew much faster and bigger than those formed without Na⁺ or Mg²⁺. Interestingly,

in previous work on the homogenous formation of Mn oxides, we found that Na⁺ increased the IS and greatly inhibited the Mn oxidation rate.¹⁹ In contrast, for the Mn oxides heterogeneously nucleated in the presence of Na⁺ or Mg²⁺, more oxides were generated at a higher IS. At 20 hr, long narrow stripes of Mn oxide became the dominant morphology. In the presence of Mg²⁺ rather than Na⁺ (Figure 5c,f), fewer Mn oxides with smaller particle sizes and heights were initially produced. Instead of narrow stripes, chains of small particles were observed at 20 hr. Thus, along with the crystalline phase evolution, the morphology of the heterogeneously formed Mn oxides also changed with time and presented differently in the presence or absence of additional Na⁺ or Mg²⁺. Note that the vertical orientation of the quartz substrates in the cuvette (Figure 1a) made it highly unlikely that the large particles were generated from homogeneously formed Mn oxides.

To clearly observe the morphologies of Mn oxides without a quartz background, heterogeneously formed Mn oxides were gently scraped from the quartz surface and placed on a TEM grid. As shown in Figure 6, samples with and without additional cations had distinctively different morphologies. Without Na⁺ or Mg²⁺, the large pieces of particles with large heights in the AFM image overlie the thin flakes in the TEM image. The edges of the thin flakes are rolled up owing to high surface tension, as previously reported. With coexisting Na⁺, Mn oxides grew taller and much faster than in the absence of cations. The narrow stripes in the AFM images are a large and thick island of Mn oxide in the TEM image. In contrast, with coexisting Mg²⁺, chains of small particles are observed in the TEM image, which match those in the AFM image. Figure S7 shows the selective area electron diffraction (SAED) patterns of Mn oxides formed at 20 hr. Without Na⁺ or Mg²⁺, the observed ring patterns suggest the heterogenous formation of amorphous phases of Mn oxides, making it difficult to identify the phases. The SAED patterns of Mn oxides formed with Mg²⁺ indicate the

formation of cryptomelane and groutite. The results are consistent with the findings by GIWAXS. However, it is worth noting that, compared with GIWAXS, SAED patterns are generally more challenging to use for phase identification, particularly for Mn oxides formed in the early stages of the reaction. In addition, the quantity of Mn oxides formed on quartz was too small to be observed with the naked eye, making it difficult to prepare heterogeneously formed Mn oxides samples for TEM.

Comparison of the Crystalline Structures of Mn Oxides Homogeneously and Heterogeneously Formed under Light Illumination. For easy comparison, Table 2 summarizes the crystalline structures of the homogeneously and heterogeneously formed Mn oxides. For the Mn oxides homogeneously formed without Na⁺ or Mg²⁺, birnessite with a layer structure was produced. ^{16,17} In the presence of Na⁺, we previously found that birnessite was also formed and Na⁺ was intercalated into the interlayer of the birnessite. ¹⁹ The increased IS caused by NaCl enhanced the crystallinity of birnessite. ¹⁹ As shown in Figure S8, in the presence of Mg²⁺, both todorokite (3×3) and birnessite were generated. Mg²⁺ was incorporated into the todorokite by interacting with Mn(III) and located at the corner of the tunnel structure, which induced the formation of todorokite. ⁵⁷⁻⁵⁹

For the Mn oxides heterogeneously formed on quartz substrates without Na⁺ or Mg²⁺, romanechite (3×2) was initially formed at 6 hr, and cryptomelane (2×2) and groutite (2×1) were newly formed at 12 and 20 hr. This is probably a consequence of one large tunnel splitting into two smaller tunnels of Mn oxides, by migrating the Mn atom from the intralayer to the interlayer to construct tunnel walls.^{60, 61} Mn-O bonds can be partially broken or weakened to enable an Mn migration.⁶⁰ The structural stability and defects of Mn oxides also affected the phase evolution process.^{62, 63} On the other hand, in the presence of Na⁺, cryptomelane (2×2) was produced first,

and gradually became romanechite (3×2) and groutellite (2×1). Two (2×2) tunnels were evolved into one bigger (3×2) and one smaller (2×1) tunnel. It possibly stems from the migration of the tunnel walls. In the presence of Mg²⁺, romanechite (3×2) was initially generated at 6 hr. Both romanechite (3 \times 2) and groutite (2 \times 1) were observed at 12 hr. By 20 hr, romanechite (3 \times 2) has disappeared and evolved to groutite (2×1) and cryptomelane (2×2). During the phase transformation process, Mn(III) can play a crucial role. Mn(III) can be formed via the comproportionation reaction between adsorbed Mn(II) and Mn(IV) in Mn oxides,64 and then adsorb at the vacant sites of Mn oxides. The Mn(III) can serve as a precursor for rapid structural rearrangement. 65 This rearrangement leads to the formation of tunnel walls in Mn oxides by sharing oxygen atoms between Mn(III) octahedra adsorbed at vacancies of adjacent layers. 65, 66 On the other hand, in the presence of Mg²⁺, Mg²⁺ can complex with Mn(III) and affect the important roles of Mn(III) in the Mn migration.⁶⁷ In addition, Mg²⁺ can stabilize the interlayer region and support the formation of large tunnel structures at the early stage of the reaction. ⁶⁰ In contrast, Na⁺ facilitates the formation of smaller tunnels than that in the presence of Mg²⁺.60 Large tunnel structures were also observed in the absence of Na⁺ or Mg²⁺, which may result from the fact that the low ionic strength of the solution promotes the kinetics of Mn oxides formation.¹⁹ Notably, although Cl radicals may have formed when Cl was added to the solution, in our previous study, we found that the addition of 500 mM Cl⁻ did not result in the generation of new crystalline structures of Mn oxides. 19 Moreover, in this study, we used much lower concentrations of Cl⁻ than in our previous study. Therefore, we believe that Cl radicals have negligible effects on the formation and transformation of Mn oxides.

293

294

295

296

297

298

299

300

301

302

303

304

305

306

307

308

309

310

311

312

313

314

315

The diverse crystalline phases of Mn oxides formed during the phase evolution processes in the presence of different cations. This finding suggests new insights into the occurrences of Mn

oxides in the environment and provides an improved understanding of the abiotic formation mechanism and diversity of natural Mn oxides. In addition, Mn oxides are promising adsorbents for pollutants in wastewater. In particular, cryptomelane was used for the adsorption of Co²⁺, Zn²⁺, Pb²⁺, and Cd²⁺.68,69 Cryptomelane and romanechite were employed as molecular sieve material.⁴¹, ⁴² An improved understanding of the nanostructures and crystallographic types of Mn oxides would go far towards explaining their adsorption affinities for heavy metal ions. ^{68, 69} Further, Mn oxides have been called a "catalytic Swiss army knife", 70 due to their important roles in catalytic reactions. Especially, cryptomelane and groutellite can function as catalyst materials. 45, 46 The structural features of Mn oxides significantly influence their catalytic selectivity and activity. 36,71 Moreover, cryptomelane and romanechite were used as battery electrode materials. 43, 44 In battery applications, the nanostructures, crystallographic types, heterogeneity, and crystal morphologies of Mn oxides greatly affect their electrochemical performance as electrode materials in energy storage. 72-74 Hence, our study can help to design a novel, environmentally friendly, and facile pathway for synthesizing specific crystallographic types of Mn oxide, and can illuminate the phase transformation of Mn oxides in these application areas.

CONCLUSION

316

317

318

319

320

321

322

323

324

325

326

327

328

329

330

331

332

333

334

335

336

337

In summary, different from studies of the photochemically-induced abiotic homogeneous formation of Mn oxides, this work showed the crystalline phase evolution and morphology changes of heterogeneously formed Mn oxides on quartz substrates over time. The presence of Na⁺ or Mg²⁺ not only affected the initial crystalline phase and phase evolution of the formed Mn oxides, but also altered their surface morphology. These findings help us understand the natural formation mechanism of diverse Mn oxides. This study also provides new insights into the

pathways for synthesizing tailored Mn oxide crystalline structures for these engineering applications.

SUPPORTING INFORMATION AVAILABLE

(S1) AFM image of the clean quartz substrate. (S2) Light spectrum of the Xenon arc lamp. (S3) Reference peak values for XPS Mn 3p. (S4) Mn oxides heterogeneously formed over 3 hr. (S5) GIWAXS characterization of the phase of the quartz substrate. (S6) XPS Mg KLL Auger spectra of heterogeneously formed Mn oxides. (S7) Selective area electron diffraction patterns of heterogeneously formed Mn oxides. (S8) XRD spectra of homogeneously formed Mn oxide solids.

ACKNOWLEDGMENTS

We are honored to be a part of the "Michael R. Hoffmann Festschrift". Prof. Hoffmann is a leading environmental chemist and engineer who pioneered the study of photochemistry in many natural and engineered environmental systems. Y.-S. Jun deeply appreciates his strong support and advice during her career and thanks him for being a generous and insightful academic grandfather. Jun and her students have been inspired by his leadership in environmental chemistry. The authors are grateful for the support received from the National Science Foundation's Environmental Chemical Sciences program (CHE-1905077). P.-I. Chou acknowledges a fellowship from the McDonnell International Scholars Academy. The authors would like to thank the Institute of Materials Science & Engineering (IMSE) of Washington University in St. Louis for the use of XPS and TEM. The use of the Advanced Photon Source (sectors 12-ID-B) at the Argonne National Laboratory was supported by the U.S. Department of Energy, Office of Science, Office of Basic Energy Sciences, under Contract No. DE-AC02-06CH11357. The authors thank Professor James C. Ballard for carefully reviewing the manuscript.

CONFLICT OF INTEREST

360

363

The authors declare that they have no known competing financial interests or personal relationships that could have appeared to influence the work reported in this paper.

364 • REFERENCES

- 1. Post, J. E., Manganese oxide minerals: Crystal structures and economic and environmental
- 366 significance. *Proc. Natl. Acad. Sci. U.S.A* **1999**, *96*, (7), 3447-3454.
- 367 2. Manning, B. A.; Fendorf, S. E.; Bostick, B.; Suarez, D. L., Arsenic(III) oxidation and
- arsenic(V) adsorption reactions on synthetic birnessite. Environ. Sci. Technol. 2002, 36, (5), 976-
- 369 981.
- 370 3. Brose, D. A.; James, B. R., Hexavalent chromium reduction by tartaric acid and isopropyl
- alcohol in Mid-Atlantic soils and the role of Mn(III, IV)(hydr)oxides. *Environ. Sci. Technol.* **2013**,
- *47*, (22), 12985-12991.
- 373 4. Villalobos, M.; Bargar, J.; Sposito, G., Mechanisms of Pb(II) sorption on a biogenic
- 374 manganese oxide. *Environ. Sci. Technol.* **2005,** *39*, (2), 569-576.
- Myers, C. R.; Nealson, K. H., Bacterial manganese reduction and growth with manganese
- 376 oxide as the sole electron acceptor. *Science* **1988**, 240, (4857), 1319-1321.
- 377 6. Schramm, V. L., Manganese in metabolism and enzyme function. Elsevier: 2012.
- 378 7. Morgan, J. J., Kinetics of reaction between O₂ and Mn(II) species in aqueous solutions.
- 379 Geochim. Cosmochim. Acta **2005**, 69, (1), 35-48.
- 380 8. Diem, D.; Stumm, W., Is dissolved Mn²⁺ being oxidized by O₂ in absence of Mn-bacteria
- 381 or surface catalysts? *Geochim. Cosmochim. Acta* **1984,** 48, (7), 1571-1573.
- 382 9. Learman, D.; Voelker, B.; Vazquez-Rodriguez, A.; Hansel, C., Formation of manganese
- oxides by bacterially generated superoxide. *Nat. Geosci.* **2011**, *4*, (2), 95-98.
- Hansel, C. M.; Zeiner, C. A.; Santelli, C. M.; Webb, S. M., Mn(II) oxidation by an
- ascomycete fungus is linked to superoxide production during asexual reproduction. *Proc. Natl.*
- 386 Acad. Sci. U. S. A. **2012**, 109, (31), 12621-12625.
- 387 11. Diaz, J. M.; Hansel, C. M.; Voelker, B. M.; Mendes, C. M.; Andeer, P. F.; Zhang, T.,
- Widespread production of extracellular superoxide by heterotrophic bacteria. Science 2013,
- 389 1237331.
- 390 12. Davies, S. H.; Morgan, J. J., Manganese(II) oxidation kinetics on metal oxide surfaces. J.
- 391 *Colloid Interface Sci.* **1989,** *129*, (1), 63-77.
- 392 13. Madden, A. S.; Hochella, M. F., A test of geochemical reactivity as a function of mineral
- size: Manganese oxidation promoted by hematite nanoparticles. Geochim. Cosmochim. Acta 2005,
- 394 *69*, (2), 389-398.
- Wehrli, B.; Friedl, G.; Manceau, A., Reaction rates and products of manganese oxidation
- 396 at the sediment-water interface. In *Aquatic Chemistry*, American Chemical Society: 1995; Vol.
- 397 244, pp 111-134.
- 398 15. Nico, P. S.; Anastasio, C.; Zasoski, R. J., Rapid photo-oxidation of Mn(II) mediated by
- 399 humic substances. Geochim. Cosmochim. Acta 2002, 66, (23), 4047-4056.
- 400 16. Jung, H.; Chadha, T. S.; Kim, D.; Biswas, P.; Jun, Y.-S., Photochemically assisted fast
- 401 abiotic oxidation of manganese and formation of δ-MnO₂ nanosheets in nitrate solution. *Chem.*
- 402 *Commun.* **2017,** *53*, (32), 4445-4448.

- 403 17. Gao, Z.; Zhang, D.; Jun, Y.-S., Does *tert*-butyl alcohol really terminate the oxidative
- activity of 'OH in inorganic redox chemistry? *Environ. Sci. Technol.* **2021**, *55*, (15), 10442-10450.
- 405 18. Gao, Z.; Liu, J.; Skurie, C.; Zhu, Y.; Jun, Y.-S., Photochemical reactions of dissolved
- organic matter and bromide ions facilitate abiotic formation of manganese oxide solids. *Water Res.*
- **2022,** *222*, 118831.
- 408 19. Gao, Z.; Skurie, C.; Jun, Y.-S., Reactive halogen radicals in saline water promote
- 409 photochemically-assisted formation of manganese oxide nanosheets. *Environ. Sci. Nano* **2022,** 9,
- 410 (10), 3756-3765.
- 411 20. Jun, Y.-S.; Kim, D.; Neil, C. W., Heterogeneous nucleation and growth of nanoparticles at
- 412 environmental interfaces. Acc. Chem. Res. 2016, 49, (9), 1681-1690.
- 413 21. Jun, Y. S.; Kendall, T. A.; Martin, S. T.; Friend, C. M.; Vlassak, J. J., Heteroepitaxial
- 414 nucleation and oriented growth of manganese oxide islands on carbonate minerals under aqueous
- 415 conditions. *Environ. Sci. Technol.* **2005**, *39*, (5), 1239-49.
- 416 22. Jun, Y.-S.; Lee, B.; Waychunas, G. A., In situ observations of nanoparticle early
- development kinetics at mineral-water interfaces. Environ. Sci. Technol. 2010, 44, (21), 8182-
- 418 8189.
- 419 23. Hu, Y.; Neil, C.; Lee, B.; Jun, Y.-S., Control of heterogeneous Fe(III) (hydr)oxide
- 420 nucleation and growth by interfacial energies and local saturations. *Environ. Sci. Technol.* **2013**,
- 421 47, (16), 9198-9206.
- 422 24. Kendall, T. A.; Na, C.; Jun, Y.-S.; Martin, S. T., Electrical properties of mineral surfaces
- 423 for increasing water sorption. *Langmuir* **2008**, *24*, (6), 2519-2524.
- 424 25. Li, Q.; Jun, Y.-S., The apparent activation energy and pre-exponential kinetic factor for
- heterogeneous calcium carbonate nucleation on quartz. Commun. Chem. 2018, 1, (1), 1-9.
- 426 26. Ray, J. R.; Lee, B.; Baltrusaitis, J.; Jun, Y.-S., Formation of iron(III) (hydr)oxides on
- 427 polyaspartate-and alginate-coated substrates: effects of coating hydrophilicity and functional
- 428 group. Environ. Sci. Technol. 2012, 46, (24), 13167-13175.
- 429 27. Jun, Y.-S.; Martin, S. T., Cobalt alters the growth of a manganese oxide film. Langmuir
- **2006,** *22*, (5), 2235-2240.
- 431 28. Jun, Y.-S.; Zhu, Y.; Wang, Y.; Ghim, D.; Wu, X.; Kim, D.; Jung, H., Classical and
- 432 nonclassical nucleation and growth mechanisms for nanoparticle formation. Annu. Rev. Phys.
- 433 *Chem.* **2022,** *73*, 453-477.
- 434 29. Bittarello, E.; Massaro, F. R.; Rubbo, M.; Costa, E.; Aquilano, D., Witherite (BaCO₃)/α-
- 435 quartz epitaxial nucleation and growth: Experimental findings and theoretical implications on
- 436 biomineralization. *Cryst. Growth Des.* **2009**, *9*, (2), 971-977.
- 437 30. Gao, Z.; Chou, P.-I.; Liu, J.; Zhu, Y.; Jun, Y.-S., Oxidative roles of polystyrene-based
- nanoplastics in inducing manganese oxide formation under light illumination. ACS Nano 2022, 16,
- 439 (12), 20238-20250.
- 440 31. Zhu, Y.; Gao, Z.; Lee, B.; Jun, Y.-S., Process-specific effects of sulfate on CaCO₃
- formation in environmentally relevant systems. *Environ. Sci. Technol.* **2022**, *56*, (12), 9063-9074.

- Webb, S. M.; Tebo, B.; Barger, J., Structural influences of sodium and calcium ions on the
- biogenic manganese oxides produced by the marine Bacillus sp., strain SG-1. Geomicrobiol. J.
- **2005,** *22*, (3-4), 181-193.
- 445 33. Wang, J.; Li, D.; Li, P.; Zhang, P.; Xu, Q.; Yu, J., Layered manganese oxides for
- formaldehyde-oxidation at room temperature: the effect of interlayer cations. RSC Adv. 2015, 5,
- 447 (122), 100434-100442.
- 34. Shen, Y.-F.; Suib, S. L.; O'Young, C.-L., Effects of inorganic cation templates on
- octahedral molecular sieves of manganese oxide. *J. Am. Chem. Soc.* **1994**, *116*, (24), 11020-11029.
- 450 35. Najafpour, M. M.; Renger, G.; Hołyńska, M.; Moghaddam, A. N.; Aro, E.-M.; Carpentier,
- 451 R.; Nishihara, H.; Eaton-Rye, J. J.; Shen, J.-R.; Allakhverdiev, S. I., Manganese compounds as
- 452 water-oxidizing catalysts: from the natural water-oxidizing complex to nanosized manganese
- 453 oxide structures. *Chem. Rev.* **2016**, *116*, (5), 2886-2936.
- 454 36. Robinson, D. M.; Go, Y. B.; Mui, M.; Gardner, G.; Zhang, Z.; Mastrogiovanni, D.;
- 455 Garfunkel, E.; Li, J.; Greenblatt, M.; Dismukes, G. C., Photochemical water oxidation by
- 456 crystalline polymorphs of manganese oxides: structural requirements for catalysis. J. Am. Chem.
- 457 *Soc.* **2013**, *135*, (9), 3494-3501.
- 458 37. Hayashi, E.; Yamaguchi, Y.; Kamata, K.; Tsunoda, N.; Kumagai, Y.; Oba, F.; Hara, M.,
- 459 Effect of MnO₂ crystal structure on aerobic oxidation of 5-hydroxymethylfurfural to 2, 5-
- 460 furandicarboxylic acid. J. Am. Chem. Soc. 2019, 141, (2), 890-900.
- 461 38. Chen, T.; Dou, H.; Li, X.; Tang, X.; Li, J.; Hao, J., Tunnel structure effect of manganese
- oxides in complete oxidation of formaldehyde. *Microporous Mesoporous Mater.* **2009**, *122*, (1-3),
- 463 270-274.
- 464 39. Fenter, P.; Sturchio, N. C., Mineral–water interfacial structures revealed by synchrotron X-
- 465 ray scattering. *Prog. Surf. Sci.* **2004**, 77, (5-8), 171-258.
- 466 40. Gibbs, R. J., Mechanisms controlling world water chemistry. *Science* **1970**, *170*, (3962),
- 467 1088-1090.
- 468 41. Liu, J.; Makwana, V.; Cai, J.; Suib, S. L.; Aindow, M., Effects of alkali metal and
- ammonium cation templates on nanofibrous cryptomelane-type manganese oxide octahedral
- 470 molecular sieves (OMS-2). J. Phys. Chem. B **2003**, 107, (35), 9185-9194.
- 471 42. Shen, X.; Ding, Y.; Liu, J.; Laubernds, K.; Zerger, R. P.; Polverejan, M.; Son, Y.-C.;
- 472 Aindow, M.; Suib, S. L., Synthesis, characterization, and catalytic applications of manganese
- 473 oxide octahedral molecular sieve (OMS) nanowires with a 2×3 tunnel structure. Chem. Mater.
- **2004,** *16*, (25), 5327-5335.
- 475 43. Poyraz, A. S.; Huang, J.; Pelliccione, C. J.; Tong, X.; Cheng, S.; Wu, L.; Zhu, Y.;
- 476 Marschilok, A. C.; Takeuchi, K. J.; Takeuchi, E. S., Synthesis of cryptomelane type α-MnO₂
- 477 (K_xMn₈O₁₆) cathode materials with tunable K⁺ content: the role of tunnel cation concentration on
- 478 electrochemistry. J. Mater. Chem. A **2017**, *5*, (32), 16914-16928.
- 479 44. Tsuda, M.; Arai, H.; Nemoto, Y.; Sakurai, Y., Electrode performance of sodium and
- lithium-type romanechite. J. Electrochem. Soc. 2003, 150, (6), A659.

- 481 45. Lemus, M. A.; López, T.; Recillas, S.; Frías, D.; Montes, M.; Delgado, J.; Centeno, M.;
- Odriozola, J., Photocatalytic degradation of 2, 4-dichlorophenoxyacetic acid using nanocrystalline
- 483 cryptomelane composite catalysts. *J. Mol. Catal. A: Chem.* **2008**, *281*, (1-2), 107-112.
- 484 46. Masunga, N.; Tito, G. S.; Meijboom, R., Catalytic evaluation of mesoporous metal oxides
- for liquid phase oxidation of styrene. Appl. Catal. A: Gen. 2018, 552, 154-167.
- 486 47. Murashov, V. V.; Demchuk, E., Surface sites and unrelaxed surface energies of tetrahedral
- 487 silica polymorphs and silicate. *Surf. Sci.* **2005**, *595*, (1-3), 6-19.
- 488 48. EPA pH. https://www.epa.gov/caddis-vol2/ph (accessed 2023-04-26).
- 489 49. Fox, R. K.; Swinehart, D. F.; Garrett, A., The equilibria of manganese hydroxide, Mn(OH)₂,
- in solutions of hydrochloric acid and sodium hydroxide. J. Am. Chem. Soc. 1941, 63, (7), 1779-
- 491 1782.
- 492 50. Jung, H.; Chadha, T. S.; Min, Y.; Biswas, P.; Jun, Y.-S., Photochemically-assisted
- synthesis of birnessite nanosheets and their structural alteration in the presence of pyrophosphate.
- 494 ACS Sustainable Chem. Eng. **2017**, *5*, (11), 10624-10632.
- 495 51. Wright, J. M.; Colling, A., Seawater: Its Composition, Properties and Behaviour:
- 496 Prepared by an Open University Course Team. Elsevier: 2013.
- 497 52. Turner, S.; Post, J. E., Refinement of the substructure and superstructure of romanechite.
- 498 Am. Mineral. 1988, 73, (9-10), 1155-1161.
- 499 53. Post, J. E.; Von Dreele, R. B.; Buseck, P. R., Symmetry and cation displacements in
- 500 hollandites: structure refinements of hollandite, cryptomelane and priderite. Acta Crystallogr. B
- 501 Struct. Cryst. Cryst. Chem. 1982, 38, (4), 1056-1065.
- 502 54. Kohler, T.; Armbruster, T.; Libowitzky, E., Hydrogen bonding and Jahn–Teller distortion
- in groutite, α -MnOOH, and manganite, γ -MnOOH, and their relations to the manganese dioxides
- ramsdellite and pyrolusite. *J. Solid State Chem.* **1997**, *133*, (2), 486-500.
- 505 55. Holder, C. F.; Schaak, R. E., Tutorial on Powder X-ray Diffraction for Characterizing
- 506 Nanoscale Materials. ACS Nano **2019**, 13, (7), 7359-7365.
- 507 56. Post, J. E.; Heaney, P. J., Neutron and synchrotron X-ray diffraction study of the structures
- and dehydration behaviors of ramsdellite and "groutellite". Am. Mineral. 2004, 89, (7), 969-975.
- 509 57. Gao, Z.; Jung, H.; Jun, Y.-S. In Abiotic photochemically-induced oxidation of aqueous
- 510 Mn²⁺ to Mn(IV) oxide solids in the presence of cations, AGU Fall Meeting Abstracts, Virtual,
- December 1-17, 2020; American Geophysical Union: Washington, DC, USA, 2020; Vol. 2020,
- 512 pp. EP059-02.
- 513 58. Gao, Z.; Jung, H.; Jun, Y.-S. In *Photochemically-facilitated formation of todorokite with*
- 514 Ca²⁺ incorporation, Abstracts of papers of the American Chemical Society, San Diego, CA,
- August 25-29, 2019; American Chemical Society: Washington, DC, USA, 2019; Vol. 258.
- 516 59. Gao, Z. Photochemical Formation Mechanisms and Applications of Mn Oxide
- Nanomaterials. Ph.D. Dissertation, Washington University in St. Louis, MO, 2022.
- 518 60. Yuan, Y.; He, K.; Byles, B. W.; Liu, C.; Amine, K.; Lu, J.; Pomerantseva, E.; Shahbazian-
- Yassar, R., Deciphering the atomic patterns leading to MnO₂ polymorphism. *Chem* **2019**, *5*, (7),
- 520 1793-1805.

- 521 61. Peng, X.; Peng, H.; Zhao, K.; Zhang, Y.; Xia, F.; Lyu, J.; Van Tendeloo, G.; Sun, C.; Wu,
- J., Direct visualization of atomic-scale heterogeneous structure dynamics in MnO₂ nanowires. ACS
- 523 Appl. Mater. Interfaces **2021**, 13, (28), 33644-33651.
- 524 62. Liu, M.; Zhao, Q.; Liu, H.; Yang, J.; Chen, X.; Yang, L.; Cui, Y.; Huang, W.; Zhao, W.;
- 525 Song, A., Tuning phase evolution of β-MnO₂ during microwave hydrothermal synthesis for high-
- 526 performance aqueous Zn ion battery. *Nano Energy* **2019**, *64*, 103942.
- 527 63. Dinh, V.-P.; Luu, T. A.; Siemek, K.; Kozlenko, D. P.; Le, K. H.; Dang, N. T.; Nguyen, T.
- 528 V.; Le Phuc, N.; Tran, T. D.; Phan, P. T.; Lo, S. T.; Hoang, K. A. T.; Dinh, T. K.; Luong, N. T.;
- Le, N. C.; Nguyen, N.-T.; Ho, T.-H.; Tran, X. D.; Tran, P. D.; Nguyen, H. Q., Crystallization
- 530 pathways and evolution of morphologies and structural defects of α-MnO₂ under air annealing.
- 531 *Langmuir* **2022**, *38*, (50), 15604-15613.
- 532 64. Elzinga, E. J., Reductive transformation of birnessite by aqueous Mn(II). *Environ. Sci.*
- 533 *Technol.* **2011,** *45*, (15), 6366-6372.
- 534 65. Yang, P.; Lee, S.; Post, J. E.; Xu, H.; Wang, Q.; Xu, W.; Zhu, M., Trivalent manganese on
- vacancies triggers rapid transformation of layered to tunneled manganese oxides (TMOs):
- 536 Implications for occurrence of TMOs in low-temperature environment. Geochim. Cosmochim.
- 537 *Acta* **2018,** *240*, 173-190.
- 538 66. Grangeon, S.; Lanson, B.; Lanson, M., Solid-state transformation of nanocrystalline
- 539 phyllomanganate into tectomanganate: influence of initial layer and interlayer structure. Acta
- 540 *Crystallographica Section B: Structural Science, Crystal Engineering and Materials* **2014,** 70, (5),
- 541 828-838.
- 542 67. Cui, H.; Liu, X.; Tan, W.; Feng, X.; Liu, F.; Ruan, H. D., Influence of Mn(III) availability
- on the phase transformation from layered buserite to tunnel-structured todorokite. Clays Clay
- 544 *Miner.* **2008,** *56*, (4), 397-403.
- 545 68. Ghoneimy, H., Adsorption of Co²⁺ and Zn²⁺ on cryptomelane-type hydrous managese
- 546 dioxide. J. Radioanal. Nucl. Chem. 1997, 223, (1-2), 61-65.
- 547 69. Feng, X. H.; Zhai, L. M.; Tan, W. F.; Liu, F.; He, J. Z., Adsorption and redox reactions of
- heavy metals on synthesized Mn oxide minerals. *Environ. Pollut.* **2007**, *147*, (2), 366-373.
- 70. Najafpour, M. M.; Hołyńska, M.; Salimi, S., Applications of the "nano to bulk" Mn oxides:
- 550 Mn oxide as a Swiss army knife. *Coord. Chem. Rev.* **2015**, *285*, 65-75.
- 551 71. Liang, S.; Teng, F.; Bulgan, G.; Zong, R.; Zhu, Y., Effect of phase structure of MnO₂
- nanorod catalyst on the activity for CO oxidation. J. Phys. Chem. C 2008, 112, (14), 5307-5315.
- 553 72. Cheng, F.; Zhao, J.; Song, W.; Li, C.; Ma, H.; Chen, J.; Shen, P., Facile controlled synthesis
- of MnO₂ nanostructures of novel shapes and their application in batteries. *Inorg. Chem.* **2006,** 45,
- 555 (5), 2038-2044.
- Toupin, M.; Brousse, T.; Bélanger, D., Influence of microstucture on the charge storage
- properties of chemically synthesized manganese dioxide. *Chem. Mater.* **2002**, *14*, (9), 3946-3952.
- 558 74. Yuan, Y.; Liu, C.; Byles, B. W.; Yao, W.; Song, B.; Cheng, M.; Huang, Z.; Amine, K.;
- Pomerantseva, E.; Shahbazian-Yassar, R., Ordering heterogeneity of [MnO₆] octahedra in tunnel-
- structured MnO₂ and its influence on ion storage. *Joule* **2019**, *3*, (2), 471-484.

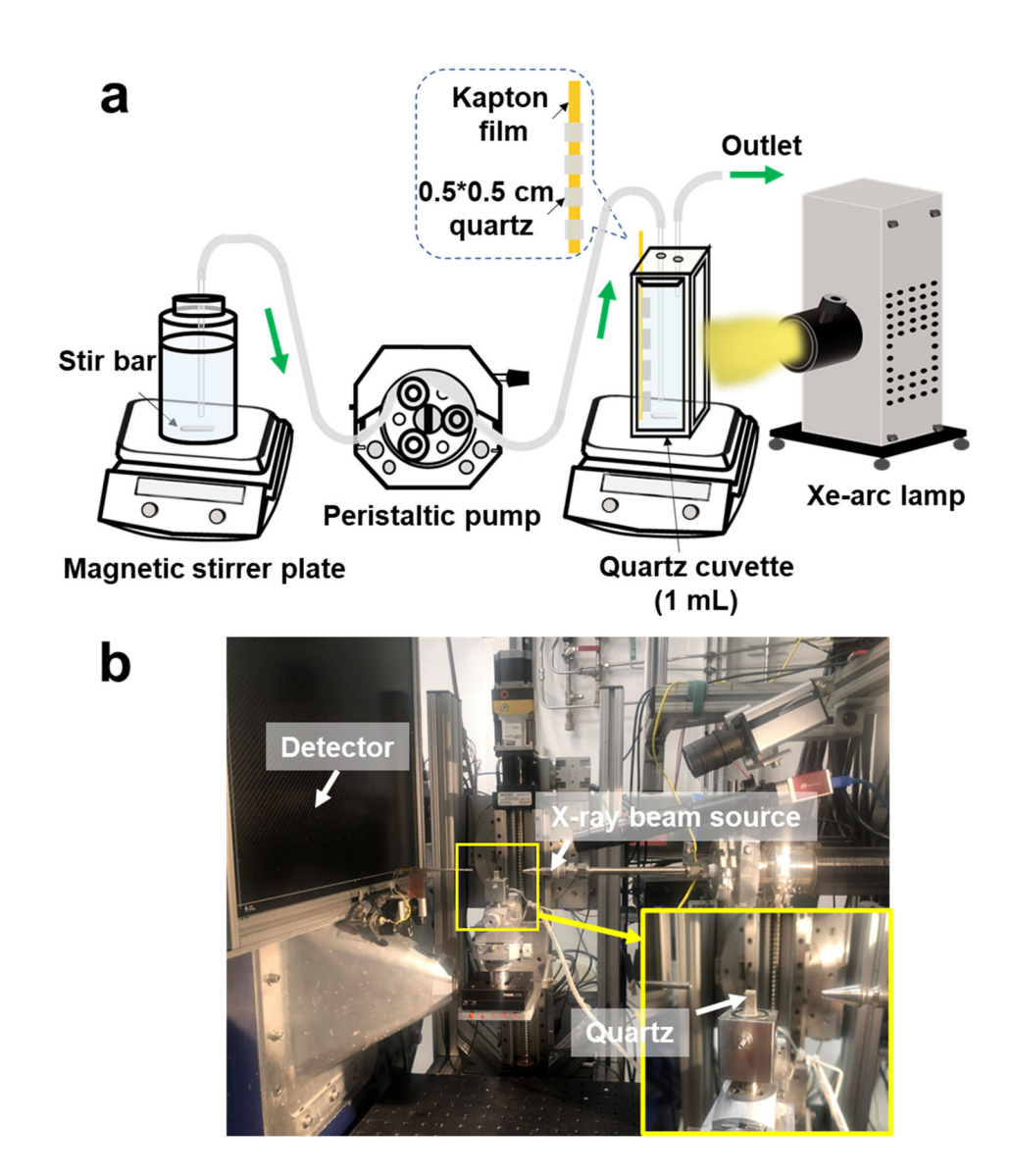


Figure 1. Schematics of (**a**) the flow-through cell for photochemically-induced heterogeneous nucleation of MnO₂ on quartz substrates and (**b**) the GIWAXS experiment setup at beamline 12-ID-B in the APS, with the quartz substrate mounted on an alignment stage shown enlarged at lower right.

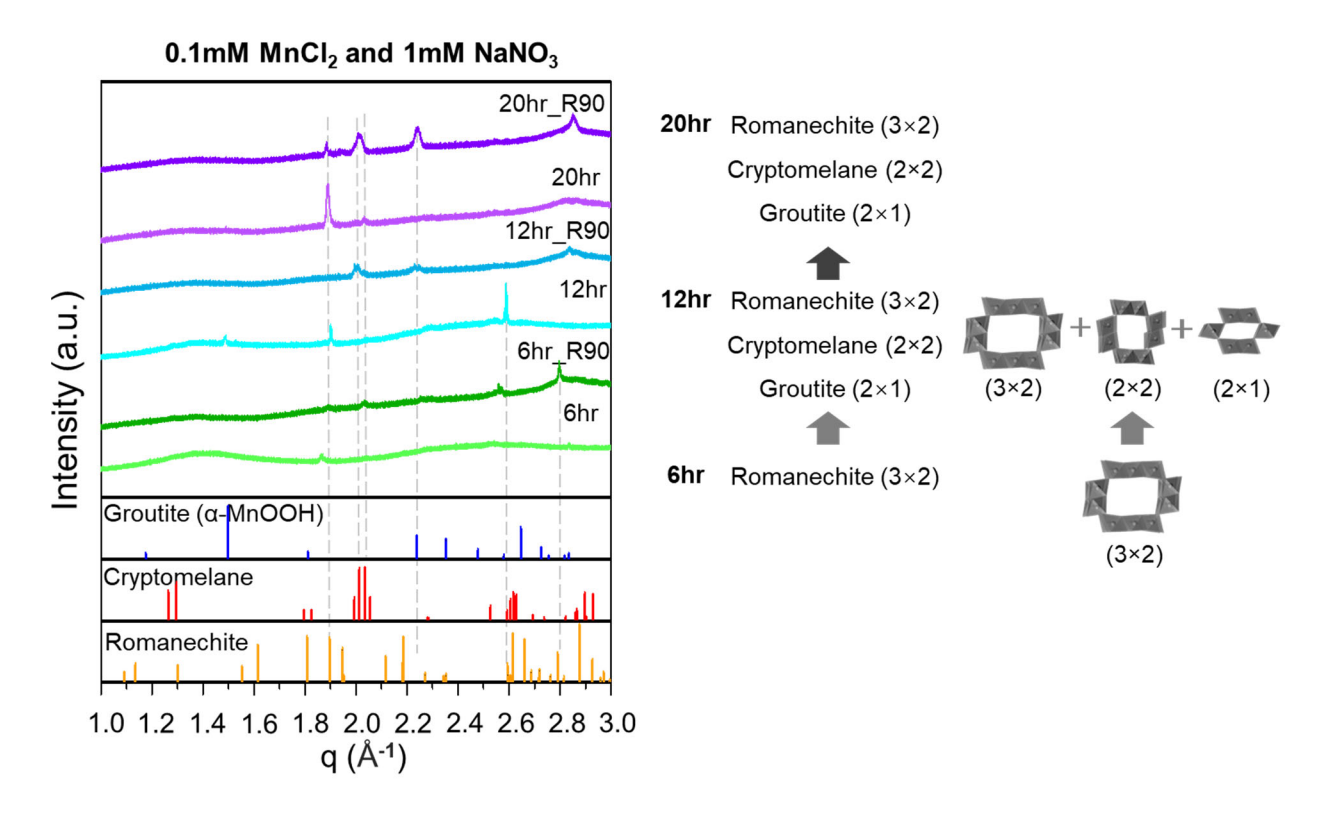


Figure 2. GIWAXS characterization of the phase of Mn oxides formed on a quartz substrate by the photolysis of solutions containing 1 mM NaNO₃ and 0.1 mM MnCl₂ at pH 9. After being measured from one orientation, the quartz substrates were rotated 90 degrees for another measurement (*e.g.*, 6hr and 6hr_R90) to get more scattering information from each sample. At least five locations on each sample were measured, and duplicate samples were prepared for each time point.

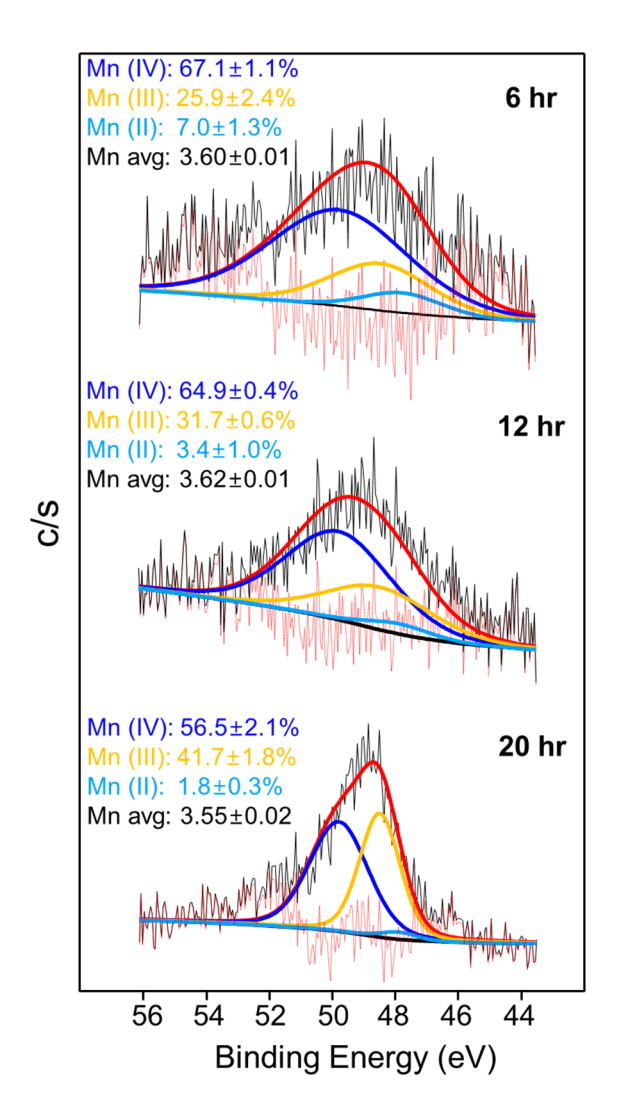
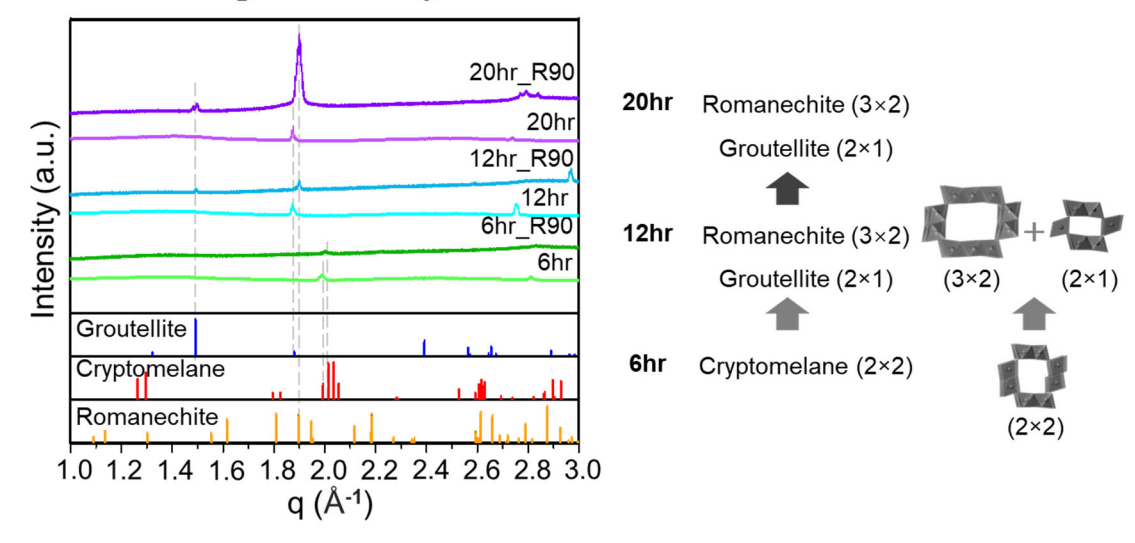


Figure 3. Average Mn oxidation states of Mn 3p spectra calculated *via* Gaussian-Lorentzian fitting of data for Mn oxides heterogeneously nucleated on a quartz substrate over time by the photolysis of solutions containing 1 mM NaNO₃ and 0.1 mM MnCl₂, at pH 9. At least duplicate samples were prepared and measured for each time point. The error ranges of the Mn(II), (III), and (IV) percentages and the Mn average oxidation state (Mn avg) were determined from the standard deviation of duplicate tests.

a 0.1mM MnCl₂, 1mM NaNO₃, and 30mM NaCl



b 0.1mM MnCl₂, 1mM NaNO₃, and 10mM MgCl₂

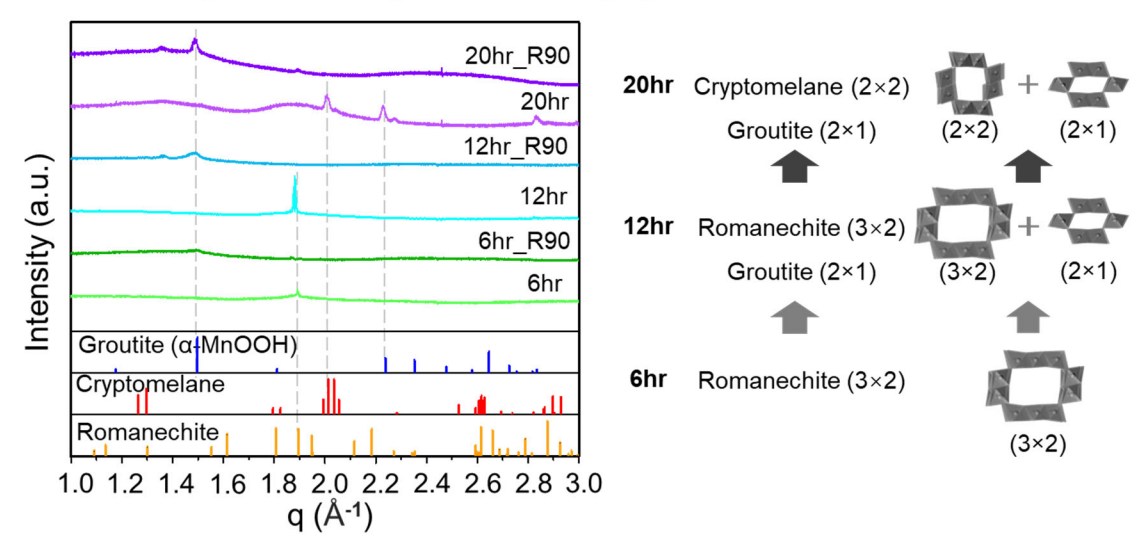


Figure 4. GIWAXS characterization of the phase of Mn oxides formed on a quartz substrate by photolysis of solutions containing 1 mM NaNO₃ and 0.1 mM MnCl₂, at pH 9, and (a) with 30 mM NaCl or (b) with 10 mM MgCl₂. At least five locations on each sample were measured, and duplicate samples were prepared for each time point.

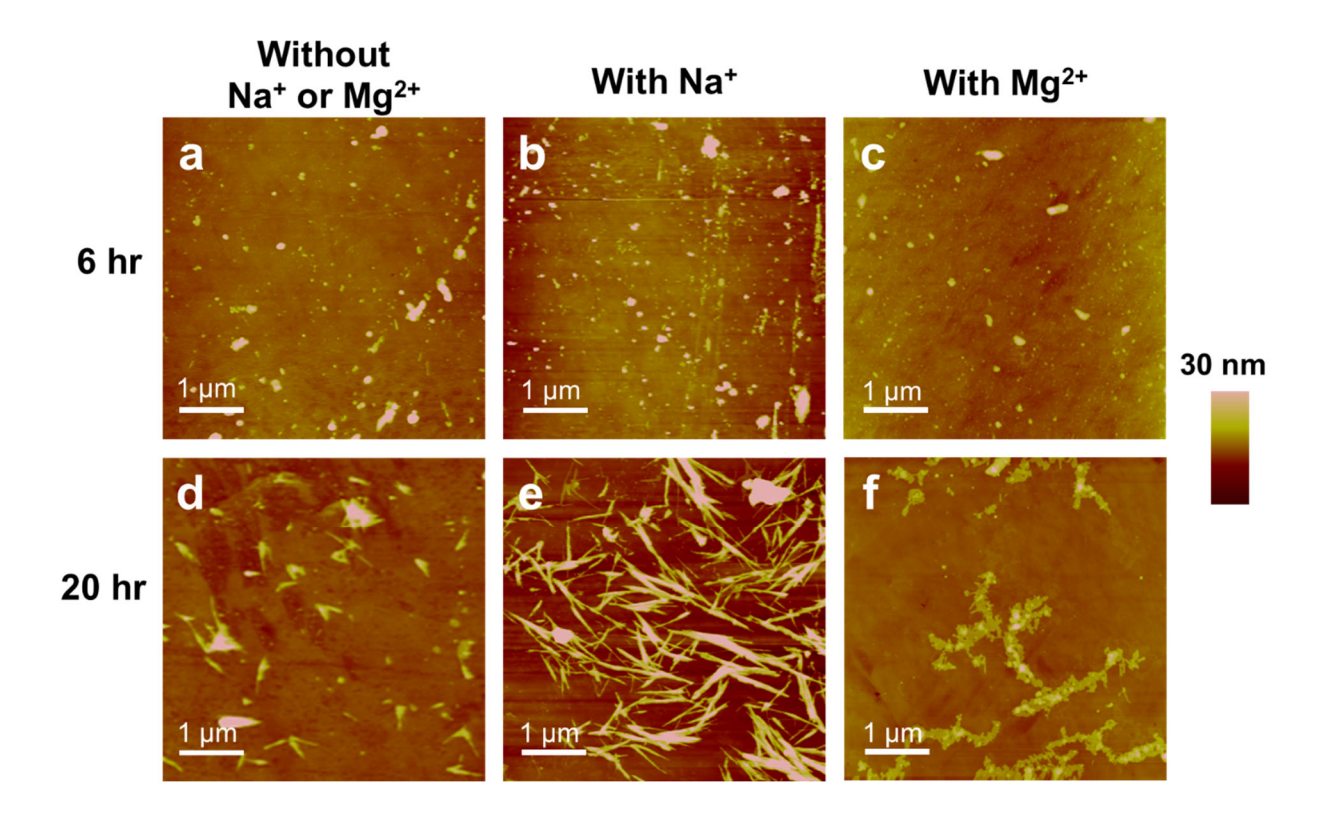


Figure 5. Representative AFM height mode images of Mn oxide heterogeneously nucleated on a quartz substrate over time. Mn oxides were formed by photolysis of solutions containing 1 mM NaNO₃ and 0.1 mM MnCl₂, at pH 9, and (a) without Na⁺ or Mg²⁺, (b) with 30 mM NaCl, or (c) with 10 mM MgCl₂ at 6 hr; (**d-f**) at 20 hr. For each sample, at least five different locations on the quartz substrates were measured.

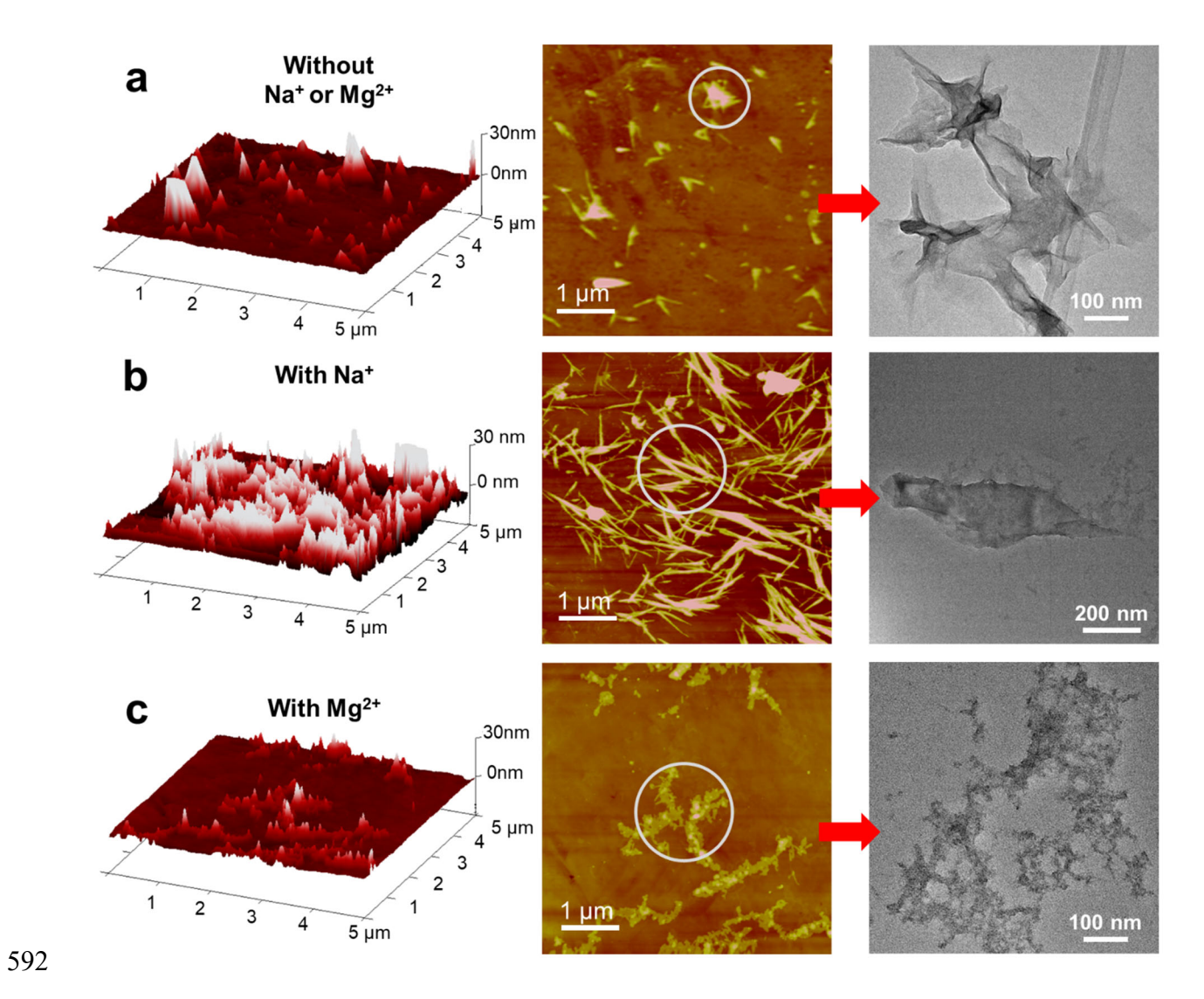


Figure 6. Comparison of the morphologies of Mn oxide heterogeneously nucleated on a quartz substrate by the photolysis of solutions containing 1 mM NaNO₃ and 0.1 mM MnCl₂, at pH 9, and (a) without Na⁺ or Mg²⁺, (b) with 30 mM NaCl, or (c) with 10 mM MgCl₂. For each TEM image, the morphology of the Mn oxides matches that in the white circle in the corresponding AFM image. For each sample, at least five different locations on the TEM grids were measured.

Table 1. Solution conditions in this study

Conditions	NaNO ₃ (mM)	MnCl ₂ (mM)	NaCl (mM)	MgCl ₂ (mM)	рН	IS (mM)
C 1	1	0.1	0	0	9.0 ± 0.1	1.3
C2	1	0.1	30	0	9.0 ± 0.1	31.3
C3	1	0.1	0	10	9.0 ± 0.1	31.3

Table 2. Summary and comparison of the crystalline phases of the homogeneously or heterogeneously nucleated Mn oxides. ^a

Conditions	No Na ⁺ or Mg ²⁺	With Na ⁺	With Mg ²⁺	
Homogeneous formation	Birnessite (layer)	Birnessite with a high crystallinity	Todorokite (3×3) and birnessite	
	(Ref. ¹⁶ and ¹⁷)	(Ref. ¹⁹)	(Fig. S8, Ref. ⁵⁷⁻⁵⁹)	
Heterogeneous formation on a quartz substrate	Romanechite (3×2)→ Romanechite (3×2) +Cryptomelane (2×2) +Groutite (2×1)	Cryptomelane $(2\times2)\rightarrow$ Romanechite (3×2) +Groutellite (2×1)	Romanechite $(3\times2)\rightarrow$ Romanechite (3×2) +Groutite $(2\times1)\rightarrow$ Groutite (2×1) +Cryptomelane (2×2)	
	(This work)	(This work)	(This work)	

^a Homogeneously or heterogeneously nucleated Mn oxides are formed by the photolysis of the solutions containing 1 mM NaNO₃, 0.1 mM MnCl₂ under pH 9, without Na⁺ or Mg²⁺; with additional Na⁺; or with additional Mg²⁺. For homogeneous nucleation conditions, because of forming Mn oxides and CO₂ adsorption into the solution, the solution pH decreased to ∼6 after 6 hr reaction.

608 TOC Graphic

